

Synthesis of $\text{LiNi}_{0.5}\text{Mn}_{1.5}\text{O}_4$ nano/microspheres with adjustable hollow structures for lithium-ion battery

Shiyu Li¹ · Shan Geng¹ · Jiachen Zhao¹ · Xiaoling Cui¹

Received: 20 June 2017 / Revised: 27 July 2017 / Accepted: 7 August 2017 / Published online: 21 August 2017
© Springer-Verlag GmbH Germany 2017

Abstract High-voltage spinel $\text{LiNi}_{0.5}\text{Mn}_{1.5}\text{O}_4$ nano/microspheres with adjustable hollow structures have been fabricated based on the Kirkendall effect. The main characteristic is that the wall thickness of the hollow structure as well as the cavity size of the hollow structure can be adjusted by the different ratio of mixed precipitation agents. Especially, the diagrammatic sketch for the formation process of various $\text{LiNi}_{0.5}\text{Mn}_{1.5}\text{O}_4$ materials with adjustable hollow structures is discussed. Besides, the results of electrochemical performance test show that $\text{LiNi}_{0.5}\text{Mn}_{1.5}\text{O}_4$ obtained from 10:1 $\text{Na}_2\text{CO}_3/\text{NaOH}$ (in mole) ratio is worth looking forward to, owing to its special hierarchical nano/microsphere and moderate hollow structures.

Keywords Lithium-ion batteries · Nano/microspheres · Kirkendall effect · Hollow structures

Introduction

The exhaustion of traditional energy and the deterioration of the environment have been seriously hindering social development and daily life, especially transportation. Exploring more efficient and environmentally friendly power devices has attracted tremendous attention. Meanwhile, numerous applications are now putting increased demands on electrical energy storage devices [1]. And among these various devices, lithium-ion batteries (LIBs) have been considered as the most promising one in terms of high voltage, large specific capacity, and

environmental friendliness [2]. To further increase the energy and power density of LIBs, one appropriate way that has received a great deal of attention is the application of cathode materials with high electrode potentials of nearly 5 V vs. Li/Li^+ , such as $\text{LiNi}_{0.5}\text{Mn}_{1.5}\text{O}_4$ spinel [3]. $\text{LiNi}_{0.5}\text{Mn}_{1.5}\text{O}_4$ spinel offers the advantages of both higher capacity and operating voltage than the manganese-only LiMn_2O_4 spinel. Besides, it is well known that $\text{LiNi}_{0.5}\text{Mn}_{1.5}\text{O}_4$ spinel has the three-dimensional Li^+ ion diffusion paths in the spinel lattice, which offers great potential for high-rate capability.

Despite improvements in electrochemical performance, ordinary $\text{LiNi}_{0.5}\text{Mn}_{1.5}\text{O}_4$ spinel without any modified strategy is struggling to meet the composite demand of developments of electric vehicles (EVs) and hybrid electric vehicles (HEVs). As high-performance batteries for large-scale electrical energy storage, in addition to high voltage, there are many other stringent requirements, such as high-rate and long-life performances. That is, based on the advantages and characteristics of the pre-modification, we should take necessary measures to further improve the rate and cycle performances of natural $\text{LiNi}_{0.5}\text{Mn}_{1.5}\text{O}_4$ spinel, in order to overcome the major obstacles in power battery applications.

In the past few years, various feasible strategies are proposed to improve rate capability for cathode materials, such as optimizing the crystalline lattice of active materials by doping cations or anions [4], reducing particles to suitable scale to offer enhanced electron/ Li^+ conductivity and reactivity [5]. Considering the fact that the functionalities of $\text{LiNi}_{0.5}\text{Mn}_{1.5}\text{O}_4$ could be adjusted efficiently by controlling their structures, many kinds of reports have been used to wish special structures to making material with different morphologies (nanoparticle [6], polyhedron [7], porous structure [8], porous nanorod [9], and so on), especially nano/microsphere structures. As we all know, hierarchical nano/microsphere structures have joined the intrinsic effect of bulk materials with the nanoeffect of

✉ Xiaoling Cui
xlcuilw@163.com

¹ College of Petrochemical Technology, School of Petrochemical Engineering, Lanzhou University of Technology, Lanzhou 730050, China

nanomaterials and produced many combinatory effects. That is, coupled with the advantages of nanometer and micrometer materials, nano/microstructures could not only bring both high surface area and short Li^+ diffusion distance to promote rate capability but also have the characteristics of anti-aggregation performance to improve cyclability.

Besides, cathode materials with hollow structures, which can lessen the compounded internal stresses and provide a more uniform current distribution of Li^+ ions [10], have attracted intensive interest for the application of LIBs in EVs and HEVs [11, 12]. As reported, the shell structure and cavity size play an important role in the electrochemical performance, described as follows: (1) the shell provides short distances for Li^+ and electron diffusion, leading to faster rate performance, and (2) the interior void space can buffer the structural strain and volume change associated with the repeated Li^+ insertion/extraction processes, thus improving the cycling stability [13, 14]. However, there is still room for improvement in hollow structured electrode materials in the particular field of LIBs, due to the fact that the shell structure and wall thickness of the hollow structure as well as cavity size should be controlled and optimized.

Herein, high-voltage spinel $\text{LiNi}_{0.5}\text{Mn}_{1.5}\text{O}_4$ nano/microspheres with hollow structures have been synthesized by a novel and simple method. The main characteristic is that the wall thickness of the hollow structure as well as cavity size of the hollow structure can be adjusted by the different ratio of two kinds of precipitation agents. Besides, the formation process and the effect on electrochemical performances of hollow structure were discussed in detail.

Experimental

Synthesis

The precursor microspheres were prepared by a precipitation method described as outlined below. Stoichiometric $\text{C}_2\text{H}_6\text{O}_4\text{Ni}\cdot 4\text{H}_2\text{O}$ and $\text{C}_4\text{H}_6\text{MnO}_4\cdot 4\text{H}_2\text{O}$ are dissolved in de-ionized water, with a mole ratio of 1:3. Then, alkaline solution was added by employment of sodium carbonate (Na_2CO_3) and sodium hydroxide (NaOH) as mixed precipitation agents at 80 °C under normal stirring conditions. The mole ratios of Na_2CO_3 and NaOH were 1:0, 25:1, 10:1, 8:1, and 5:1, respectively. And pH of each mother solution is controlled in the range of 8–8.5. After being filtrated and washed, the five types of precipitates were dried at 80 °C for 12 h and sintered at 450 °C for 10 h, respectively.

Then, the as-obtained precursor powders were immersed in stoichiometric $\text{CH}_3\text{COOLi}\cdot 2\text{H}_2\text{O}$ alcohol solution at 70 °C for 5 h, with a molar ratio of $\text{Li}/\text{Ni}/\text{Mn} = 1.0:0.5:1.5$. After evaporation in vacuum, the yielded powders were dried at 120 °C for 2 h and sintered at 800 °C for 10 h. The final products got from

the different starting precipitation agents are labeled as LNMO-A, LNMO-B, LNMO-C, LNMO-D, and LNMO-E, respectively.

Characterization

Structures of samples were characterized by X-ray diffraction (XRD; D/max-2400, Japan) with $\text{Cu K}\alpha$ radiation, a tube voltage of 30 kV, a tube current of 100 mA, and a step size of $0.02^\circ \text{ s}^{-1}$ over range of 10° to 120° . The morphology and composition of samples were determined under scanning electron microscopy (SEM, JSM-5600, Japan) and transmission electron microscopy (TEM, FEI Tecnai G2 F20, USA).

The mixture of $\text{LiNi}_{0.5}\text{Mn}_{1.5}\text{O}_4$ active materials (80%), conductive acetylene black as a conductive agent (10%), and polyvinylidene fluoride (PVDF) (10%) as a binder was dissolved in *N*-methyl pyrrolidinone. The slurry was coated onto an aluminum foil and then dried in a vacuum oven at 120 °C for 12 h to prepare $\text{LiNi}_{0.5}\text{Mn}_{1.5}\text{O}_4$ cathode film.

Electrochemical performances of samples were tested with experimental coin cells (CR2032 type) of $\text{LiNi}_{0.5}\text{Mn}_{1.5}\text{O}_4/\text{Li}$, by LAND CT2001A tester (Wuhan, China) in the voltage range of 3.5–5 V. Cells were assembled in an argon atmosphere glove box, using a lithium sheet as the anode material, the above prepared electrode as the cathode material, 1 M LiPF_6 -ethylene carbonate/dimethyl carbonate (1:1, v/v) as a nonaqueous electrolyte and a Celgard (2400) porous polypropylene as the separator, respectively.

Electrochemical impedance spectroscopy (EIS) spectra were performed using a CHI660C Electrochemical Workstation (Shanghai, China) over a frequency range of 100 kHz to 0.01 Hz with amplitude of 10 mV.

Results and discussion

XRD patterns of $\text{LiNi}_{0.5}\text{Mn}_{1.5}\text{O}_4$ samples which can be readily indexed to the cubic spinel structure are shown in Fig. 1. Each of the samples prepared with various ratios of Na_2CO_3 and NaOH is assigned to the space group of $\text{P4}_3\text{32}$ symmetry due to the appearance of the weak peaks located at 2θ of $\sim 15.7^\circ$, 39.7° , 45.7° , and 57.5° , which conforms to JCPDS card (No. 49-0207) in the XRD patterns [15]. And no obvious impurity phase can be detected in any sample. Strong and narrow diffraction peaks for every sample indicate that all of the as-obtained $\text{LiNi}_{0.5}\text{Mn}_{1.5}\text{O}_4$ materials have good crystallinity and ordered spinel structure.

It has been widely demonstrated that crystallite size of cathode material is an important factor for the interfacial stability. And the Scherrer equation is used in the determination of size of particles of crystals in the form of powder. As we all know, the Scherrer equation, in X-ray diffraction and crystallography, is a formula that relates the size of sub-micrometer particles, or crystallites, in a solid to the broadening of a peak in a diffraction

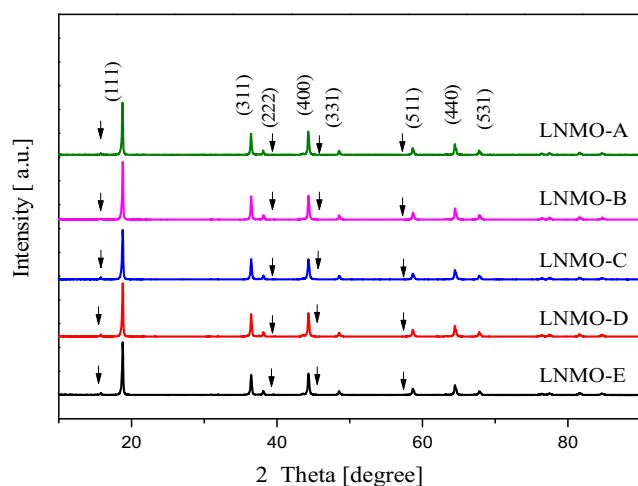


Fig. 1 XRD patterns of samples

pattern. The approximate crystallite sizes of the samples prepared with various ratios of Na_2CO_3 and NaOH are 49.3, 47.5, 45.7, 47.4, and 49.1 nm for LNMO-A, LNMO-B, LNMO-C, LNMO-D, and LNMO-E, respectively. These small crystallite sizes are attractive due to the fact that the power output of LIBs can be notably increased by reducing the particle size due to the shorter Li^+ diffusion pathways.

Figure 2 shows morphologies of precursor precipitates after sintering at 450°C . The high-magnification SEM images (Fig. 2, A1–E1) indicate that a single sphere is made up of many nanoparticles by self-assembly. And from the low-magnification SEM images (Fig. 2, A2–E2), it can be seen that the particle size decreases gradually from Fig. 2, A2–E2, with the tendency of aggregation as the increase of surface energy. It is notable that every sample shows a hollow structure in Fig. 2, due to a slight Kirkendall effect at 450°C (the Kirkendall effect will be discussed in detail in the next section). And Fig. 2 (B2) as a representative of SEM image is chosen as a typical sample to demonstrate the clear boundary between the core and the solid sphere shell.

The morphology and particle size of products are examined by SEM, as shown in Fig. 3 with the good structural inheritance of Fig. 2. As can be seen from Fig. 3, the nanoparticles with uniform size are integrated into the microspheres, forming a nano/microsphere structure. This nano/microcombination circumvented the aggregation issue that had been troubling the nanoparticles. That is, the nano/microstructure can exploit its strong points of nanoparticles for power property due to the large contacting area between the electrode and electrolyte, and avoid exposing its weaknesses of nanoparticles for cycle stability due to the destruction on structure and phase stability.

Besides, cathode materials with hollow structures can be formed by self-assembly, as captured and marked in Fig. 3 (A–C). As reported, the shell structure and cavity size play a positive role in the electrochemical performance. Interestingly, the structure of material becomes loose, and the wall thickness of the

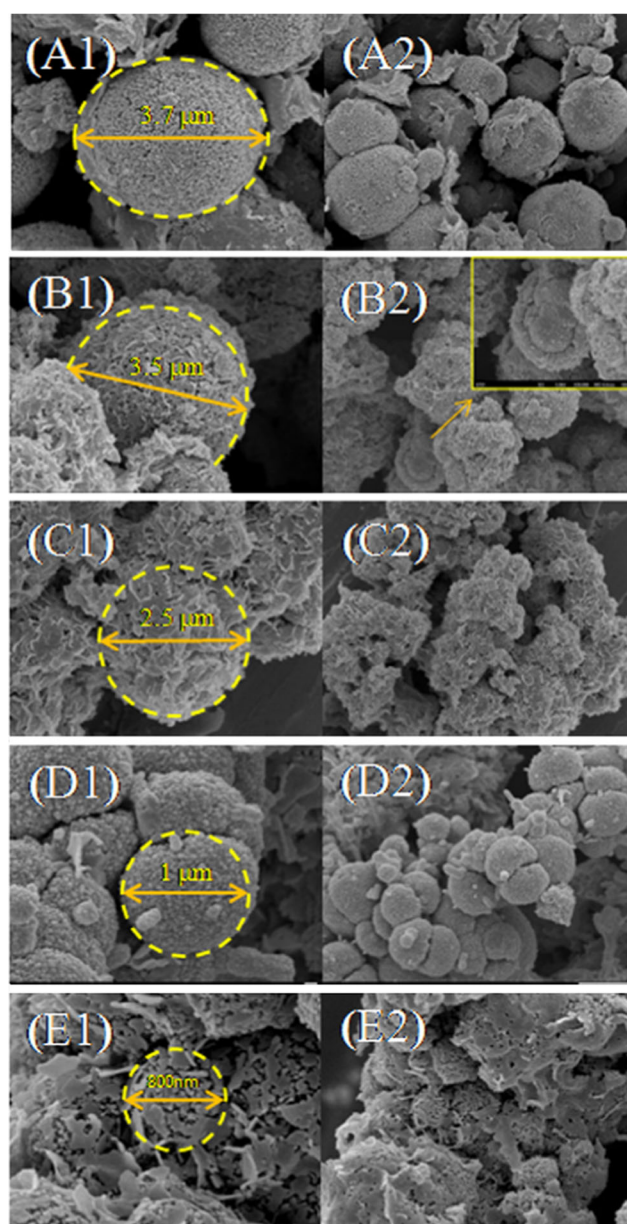
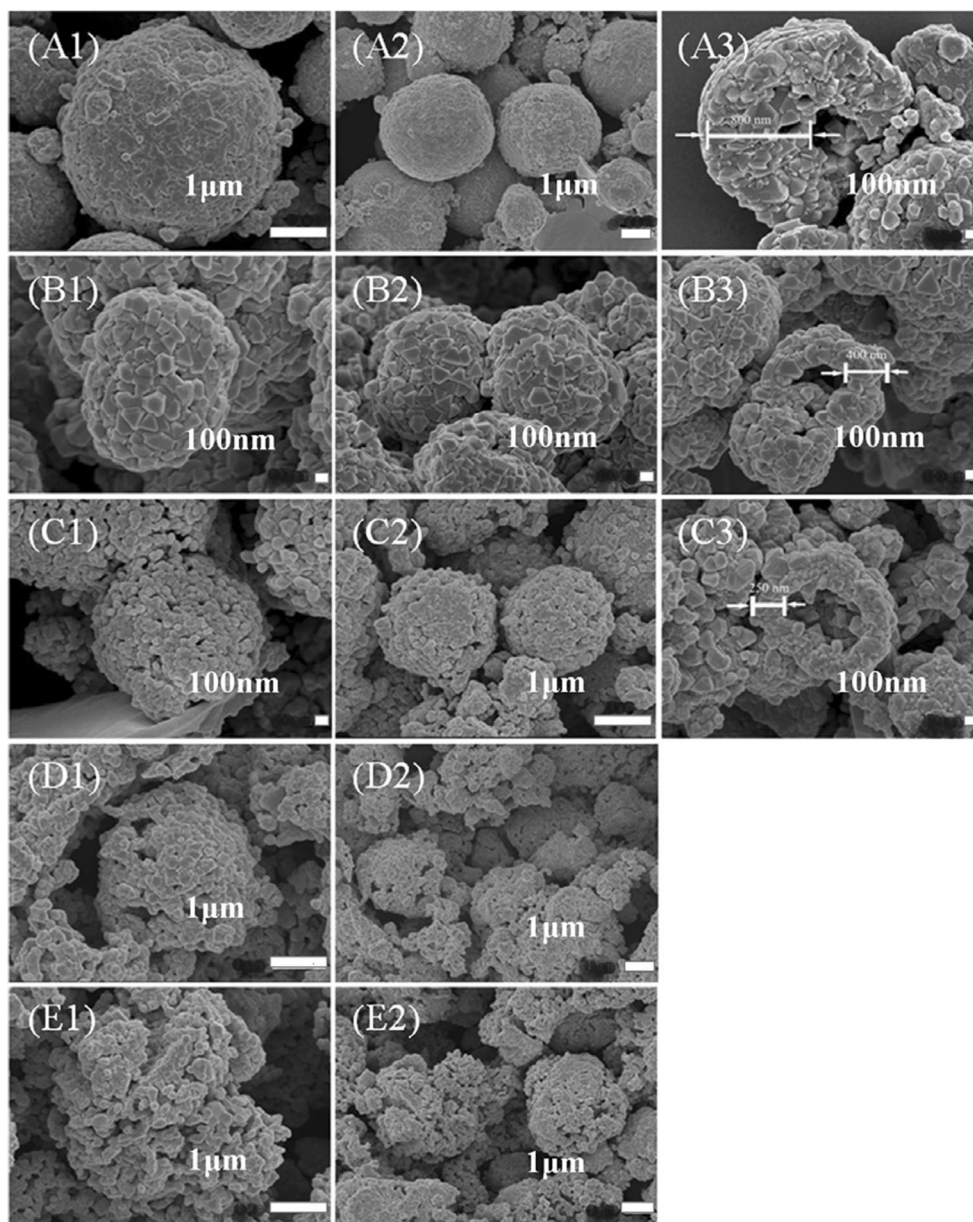


Fig. 2 SEM images of precursor precipitates after sintering at 450°C for LNMO-A (A1, A2), LNMO-B (B1, B2), LNMO-C (C1, C2), LNMO-D (D1, D2), and LNMO-E (E1, E2), respectively

surface is decreasing with an increase in the proportion of NaOH . In other words, shell structure and wall thickness of the hollow structure as well as cavity size could be controlled and optimized by the addition of moderate NaOH in Na_2CO_3 precipitation agent. And until the molar ratio of Na_2CO_3 and NaOH is less than or equal to 8, the structure of the material becomes irregularly spherical. As shown in Fig. 3 (D, E), the wall thicknesses of LNMO-D and LNMO-E materials are not marked in the cross-sectional drawings, due to the fact that the spherical structure is subjected to destruction. This may be attributed to the following two reasons, (1) given the experimental indication that the carbonate sediment is conducive to exhibit spherical particle than NaOH , and (2) the structure shrinkage should also

Fig. 3 The morphology and particle size of products: A1, A2, and A3 for LNMO-A; B1, B2, and B3 for LNMO-B; C1, C2, and C3 for LNMO-C; D1 and D2 for LNMO-D; and E1 and E2 for LNMO-E



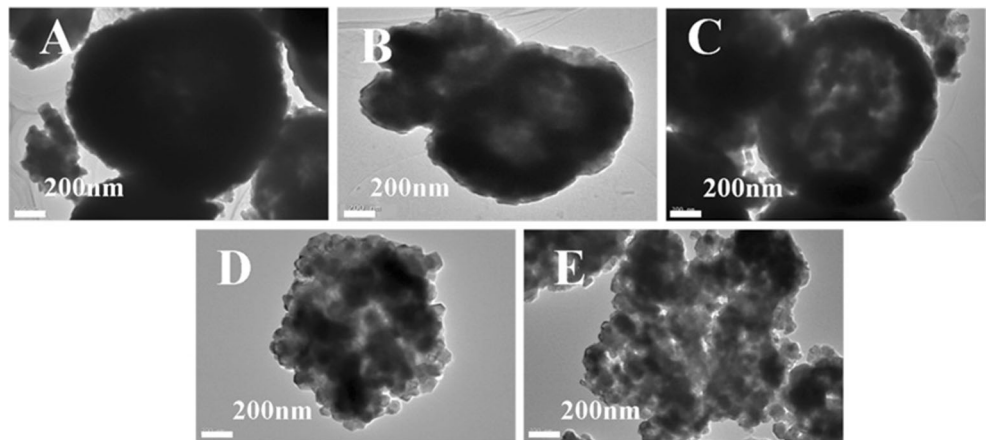
be considered which accelerated the diffusion rate of the core substance to the shell [16]. Expressly, LNMO-C is composed of uniform and intact nano/microspheres with surface hole. It should be concluded that LNMO-C would have excellent power and circulation performances.

Figure 4 shows the typical TEM images of various $\text{LiNi}_{0.5}\text{Mn}_{1.5}\text{O}_4$ materials. As expected, images of Fig. 4a–c show well-spherical hollow structures in ascending order of hollow size, and images of Fig. 4d, e show irregular shape with loose structure. Besides, it is easy to find out that the cavity inside becomes larger from LNMO-A to LNMO-E. It can also be observed that the wall thickness of samples becomes thin from LNMO-A to LNMO-E. This change of structure will affect the electrochemical properties of the materials.

The schematic procedure for the preparation of $\text{LiNi}_{0.5}\text{Mn}_{1.5}\text{O}_4$ hollow microspheres is shown in Fig. 5. Monodisperse microspheres prepared by a precipitation method are utilized as the precursors. We divide the responses into two categories, a precipitation agent that does not contain NaOH and a precipitation agent containing NaOH, which are labeled as SC and SCH, respectively. And the as-synthesized precursor of $\text{Mn}_{0.25}\text{Ni}_{0.75}(\text{CO}_3)_x(\text{OH})_{2-2x}$ (The range of x is 0.9–1, which are obtained by the proportion of Na_2CO_3 and NaOH.) powders is written in the form of co-precipitated mixture of $x\text{Ni}_{0.25}\text{Mn}_{0.75}\text{CO}_3$ and $(1-x)\text{Ni}_{0.25}\text{Mn}_{0.75}(\text{OH})_2$ for illustrative purposes only.

It is believed that chemical co-precipitation is a process of competition between crystal nucleation and crystal growth, which has a great relationship with the particle size. The

Fig. 4 TEM images of LNMO-A (a), LNMO-B (b), LNMO-C (c), LNMO-D (d), and LNMO-E (e) materials



empirical formula for nucleation rate of crystal during co-precipitation could be described as:

$$I = k \exp \left\{ -\frac{16}{3} \pi \sigma_{s-1}^3 M^2 / \rho^2 (RT)^3 \left[\ln^S / S_0 \right] \right\} \quad (1)$$

in which I denotes nucleation rate, k denotes proportionality constant, σ_{s-1} denotes solid-liquid surface tension, ρ denotes density of crystalline substance, M denotes molar mass of

crystalline materials, T denotes absolute temperature, S denotes the concentration of supersaturated solution, and S_0 denotes saturation of solution. The increase of supersaturation S/S_0 is helpful to improve the nucleation rate of crystal I . And both of the crystal nucleation rate and the crystal growth rate should be controlled during co-precipitation process to prepare particles with uniform particle size distribution and regular morphology.

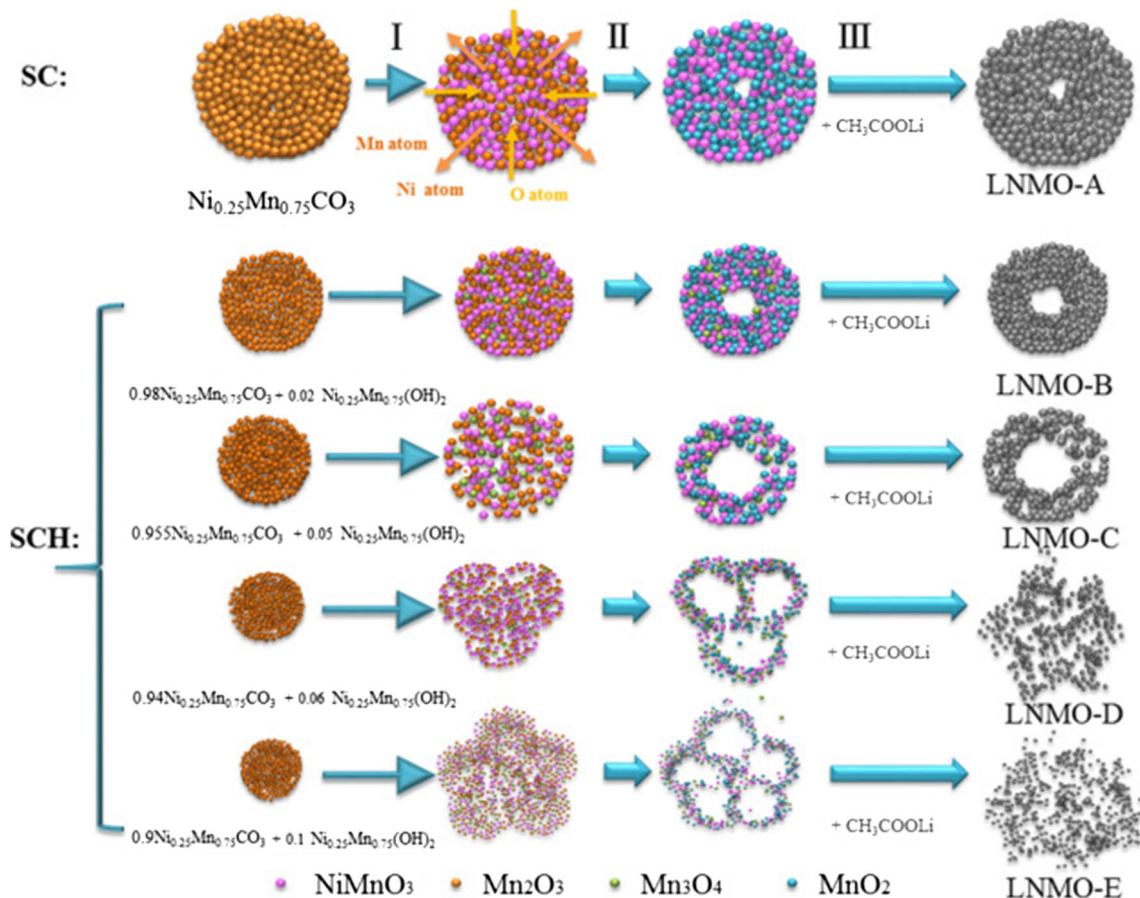


Fig. 5 The schematic diagram of formation process of $\text{LiNi}_{0.5}\text{Mn}_{1.5}\text{O}_4$ with adjustable hollow structures

At the beginning of the co-precipitation process, the crystal growth rate is less than the nucleation rate, resulting in a large number of primary particles with small size. Next, these primary particles are easy to agglomerate and form secondary particles under stirring. And the as-produced secondary particle formed can further reunite with other aggregates or primary particles to grow them. This process could be described as follows: (i) fluid motion drives particles collide, (ii) different particles close to each other van der Waals force, and (iii) adjacent particles solidified into a whole by producing chemical bonds at crystal growth and Ostwald ripening process. It is believed that nucleation is dominant during the formation of primary particle, and agglomeration is the key factor in the formation of the secondary particle. So, the control of supersaturation for reaction solution is crucial for primary particles as well as secondary particle characteristics [17].

During co-precipitation process to obtain $x\text{Ni}_{0.25}\text{Mn}_{0.75}\text{CO}_3$ and $(1-x)\text{Ni}_{0.25}\text{Mn}_{0.75}(\text{OH})_2$ mixture, the saturation of the metal salt solution decreases with increasing concentration of OH^- by the addition of NaOH precipitant. As a result, the particle size will decrease as the decline of S/S_0 . This result is consistent with SEM images obtained from Fig. 2.

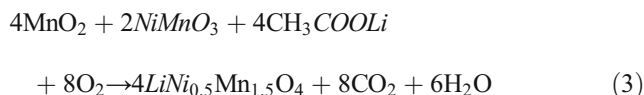
Besides, the Kirkendall effect, which was usually proposed to have responsibility for the formation of voids, provides a mechanism for void formation near interfaces due to different interdiffusion rates in a bulk diffusion couple [18]. And two probable reasons are responsible for the formation of the hollow cavity, (1) a mechanism analogous to the Kirkendall effect and (2) fusion of the mesopores in microspheres [19]. Meanwhile, the cavity becomes large and wall thickness becomes thin with the increase of the content of NaOH. It is believed that the oxidation of hydroxide is the cause of sharp contraction, leading to severe contraction structure exacerbated by the Kirkendall effect [20]. Besides, the decrease of spherical particle size is considered to be one of the main reasons with the increase of the content of NaOH.

In step I for SC, as has been corroborated by other researchers, the as-synthesized $\text{Mn}_{0.25}\text{Ni}_{0.75}\text{CO}_3$ microspheres are converted to a mixed porous oxide composed of two stable phases, NiMnO_3 and Mn_2O_3 , by thermal decomposition in the temperature range of 240–500 °C via the following reaction [21, 22],

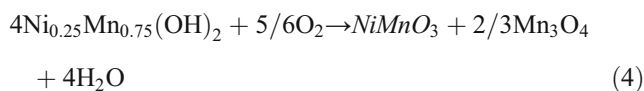


Then, the formed Mn_2O_3 is apt to transform into MnO_2 in step II ($2\text{Mn}_2\text{O}_3 + \text{O}_2 \rightarrow 4\text{MnO}_2$), due to the fast diffusion of Mn (III) atom in Mn_2O_3 . The dissociated O atoms diffuse through the gas-solid interface and oxidize half Mn^{3+} to Mn^{4+} ; meanwhile, Mn^{3+} and Ni^{2+} diffuses toward the gas-solid interface. The diffusion rate of the Mn atom and Ni atom (at the core) is faster than that of O atom (at the shell), leading to the formation of void at the core.

Next, in the last step of III, with the addition of starting lithium salt of CH_3COOLi , high-voltage spinel $\text{LiNi}_{0.5}\text{Mn}_{1.5}\text{O}_4$ nano/microspheres with hollow structures have been fabricated via the following reaction,



There are some differences between SC and SCH. For SCH in step I, in addition to the NiMnO_3 and Mn_2O_3 , some Mn_3O_4 are generated with the oxidization of $\text{Ni}_{0.25}\text{Mn}_{0.75}(\text{OH})_2$ via the following reaction,



And with the increase of NaOH content, more and more Mn_3O_4 are formed. But in our opinion, this is not the main reason for the difference on images, though it could be used to describe the formation process of hollow structures. As mentioned above (Figs. 3 and 4), obvious hollow structures could be captured only for LNMO-A, LNMO-B, and LNMO-C. Based on our study, we deduce that the spherical structure has been subjected to destruction for LNMO-D and LNMO-E, starting from the formation of co-prepared $x\text{Ni}_{0.25}\text{Mn}_{0.75}\text{CO}_3$ and $(1-x)\text{Ni}_{0.25}\text{Mn}_{0.75}(\text{OH})_2$ precipitate mixtures—illustrated by the formation case of LNMO-C and LNMO-D. As shown in Fig. 2, the particle size of LNMO-D is slightly smaller than that of LNMO-C. It means that the precursor of LNMO-D will basically undergo more violent shape change in step II with less resistance to gas release, leading to a looser and more irregular morphology, compared with LNMO-C. Such small particle size and porous structure will accelerate the diffusion rate of the core substance to the shell, and slow that of the shell to the core, being conducive to the Kirkendall effect [23]. And when this effect accumulated to a certain extent, the wall is collapsed, and the gas-solid interface is disappeared [24], corresponding to the incompact powder images captured in Fig. 3 (D, E) for LNMO-D and E.

Moreover, we have studied the effects of the synthesis method on the electrochemical performance of $\text{LiNi}_{0.5}\text{Mn}_{1.5}\text{O}_4$ cathode materials. The initial charge/discharge curves of the samples are given in Fig. 6a. For cells based on this series of five $\text{LiNi}_{0.5}\text{Mn}_{1.5}\text{O}_4$ cathode materials, every cell can deliver a discharge capacity of about 110.1, 113.9, 120.0, 120.0, and 108.8 mAh g^{-1} at a rate of 0.2 C, respectively. And the discharge curves of the samples present a relatively obvious plateau in the potential region around 4.0 V (corresponding to the redox couples of $\text{Mn}^{3+}/\text{Mn}^{4+}$), which indicates that the a little oxygen deficiency still exists due to the oxygen at high calcination temperature for long reaction time.

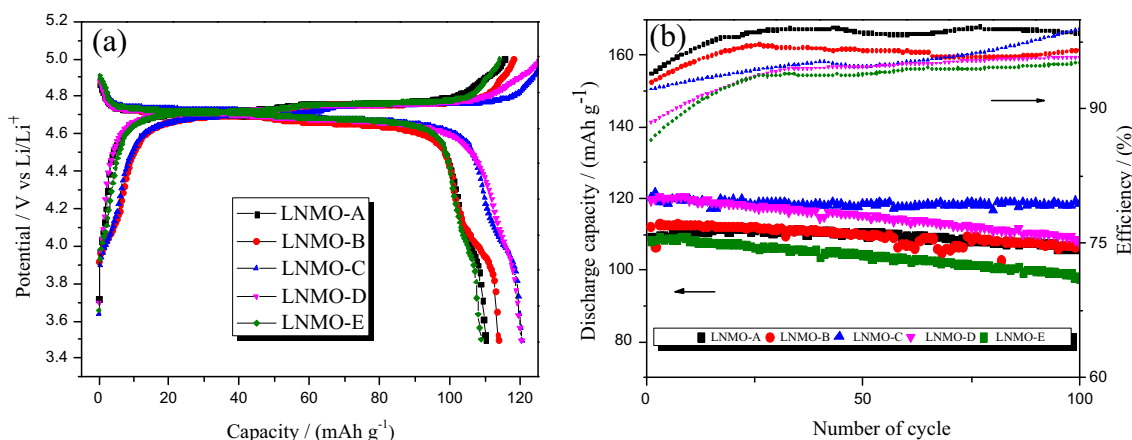


Fig. 6 The initial charge/discharge curves of the samples at 0.2 C (a). Cycling performance and coulombic efficiency of this series of $\text{LiNi}_{0.5}\text{Mn}_{1.5}\text{O}_4$ materials (b)

Cycling performance is also of great importance for powering lithium-ion batteries. Figure 6b shows cycling performance and coulombic efficiency of this series of $\text{LiNi}_{0.5}\text{Mn}_{1.5}\text{O}_4$ materials in the voltage range of 3.5–5.0 V at 0.2 C during the first 100 cycles. It can be observed that the coulombic efficiency is improved with the increase of cycle number, which is due to the electrolyte slowly penetrating into the material during the battery cycle. The electrode material is fully activated, and material utilization has been improved. In addition, it is easy to find out the regularity for capacity retention rate, with the trend shown as follows: LNMO-E < LNMO-D < LNMO-C < LNMO-B < LNMO-A. That is, only LNMO-C could show a unique balance of property, taking the discharge density and capacity fading factor into account. This result agrees with the deduction obtained from Fig. 3. And the adverse effect of the capacity fading for LNMO-D and LNMO-E is the increased contact area between acid-containing electrolyte and $\text{LiNi}_{0.5}\text{Mn}_{1.5}\text{O}_4$ -base cathode electrode to aggravate dissolution and corrosion behavior.

The rate capability of spinel $\text{LiNi}_{0.5}\text{Mn}_{1.5}\text{O}_4$ is carried out for its extended applications, such as EVs or HEVs. The discharge capacities at various rates are given in Fig. 7a. The cell was

charged and discharged at different C rates from 0.5 to 10 C. As was expected, LNMO-C and D show high-capacity retention rate, especially at a high discharge rate. For example, LNMO-C sample delivers capacity of 97.3 mAh g^{-1} at a rate of 6 C. And the LNMO-D sample delivers capacity of 93.6 mAh g^{-1} at a rate of 6 C. At a high rate of 10 C, LNMO-C (89.2 mAh g^{-1}) exhibit greater discharge capacity than LNMO-D (79.7 mAh g^{-1}).

Figure 7b shows the impedance spectra (Nyquist plots) of this series of $\text{LiNi}_{0.5}\text{Mn}_{1.5}\text{O}_4/\text{Li}$ cells after 5 cycles under 0.2 C at room temperature, which has been fitted by an equivalent circuit also shown in Fig. 7b. All of the five materials exist in two semicircles, the first one at the high-frequency region that can be assigned to the resistance of SEI layer; meanwhile, the second semicircle at the middle-frequency region reflects the charge transfer resistance. By the fitting results, LNMO-C shows the lowest resistance value, indicating conductive and stable interfacial behaviors. From LNMO-A to C, the resistance of de-intercalation and re-intercalation of Li^+ ions decreases with the short diffusion distance of Li^+ ions. However, the impedance will become large after this point of NaOH content, owing to the serious irregular agglomeration.

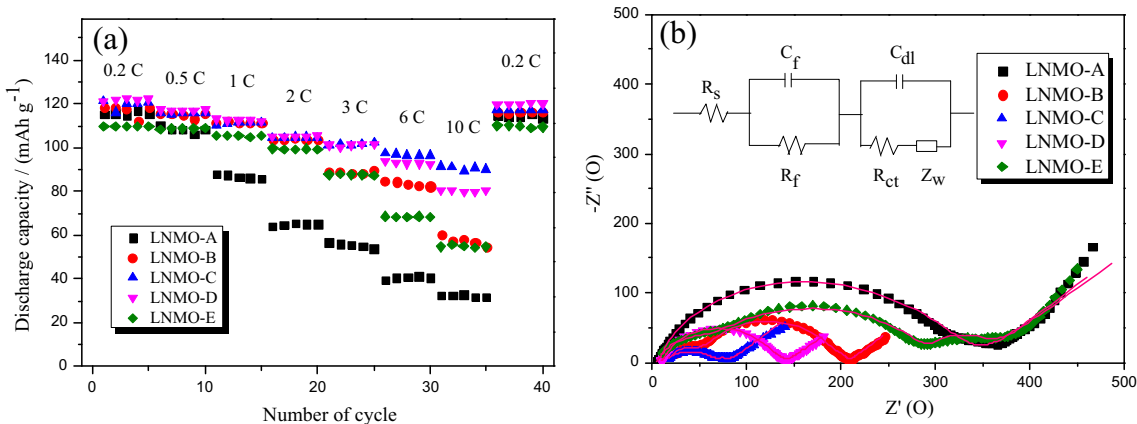


Fig. 7 The discharge capacities at various rates (a) and the EIS of this series of $\text{LiNi}_{0.5}\text{Mn}_{1.5}\text{O}_4/\text{Li}$ cells (b)

Conclusions

This work presents a simple way of preparing high-voltage spinel $\text{LiNi}_{0.5}\text{Mn}_{1.5}\text{O}_4$ nano/microspheres with hollow structures. The main characteristic is that the wall thickness of hollow structure as well as cavity size of the hollow structure can be adjusted by the different ratio of precipitation agents (Na_2CO_3 and NaOH). That is, the shell structure and the wall thickness of the obtained $\text{LiNi}_{0.5}\text{Mn}_{1.5}\text{O}_4$ materials can be adjusted from the addition of a small amount of NaOH co-precipitation agent. Especially, the diagrammatic sketch for formation process of various $\text{LiNi}_{0.5}\text{Mn}_{1.5}\text{O}_4$ materials with adjustable hollow structures has been discussed. Besides, the results of the electrochemical performance test show that, as expected, LNMO-C with hierarchical nano/microsphere and moderate hollow structures has a good ability to attract intensive interest for the application of LIBs in EVs and HEVs. We hope that the results of this study and the associated preparative technique will contribute to the search for optimum cathode material with long cycle life and high power density in advanced LIBs.

Acknowledgements The authors acknowledge the financial support from the Natural Science Foundation of China (Nos. 51502124 and 21406100).

References

- Kozawa T, Murakami T, Naito M (2016) Insertion of lattice strains into ordered $\text{LiNi}_{0.5}\text{Mn}_{1.5}\text{O}_4$ spinel by mechanical stress: a comparison of perfect versus imperfect structures as a cathode for Li-ion batteries. *J Power Sources* 320:120–126
- Su L, Jing Y, Zhou Z (2011) Li ion battery materials with core-shell nanostructures. *Nano* 3:3967–3983
- Zhang M, Wang J, Xia Y, Liu Z (2012) Microwave synthesis of spherical spinel $\text{LiNi}_{0.5}\text{Mn}_{1.5}\text{O}_4$ as cathode material for lithium-ion batteries. *J Alloys Compd* 518:68–73
- Zeng Y, Qiu K, Yang Z, Zhou F, Xia L, Bu Y (2016) Influence of europium doping on the electrochemical performance of $\text{LiNi}_{0.5}\text{Co}_{0.2}\text{Mn}_{0.3}\text{O}_2$ cathode materials for lithium ion batteries. *Ceram Int* 42:10433–10438
- Cui XL, Li YL, Li SY, Li LX, Liu JL (2013) Nanosized $\text{LiNi}_{0.5}\text{Mn}_{1.5}\text{O}_4$ spinels synthesized by a high-oxidation-state manganese sol-gel method. *Ionics* 19:1489–1494
- H. M. Cho, M. V. Chen, A. C. Macrae, Y. S. Meng (2015) Effect of surface modification on nano-structured $\text{LiNi}_{0.5}\text{Mn}_{1.5}\text{O}_4$ spinel materials, *ACS Appl Mater Interfaces*. 7:16231–16239
- Chen Z, Zhao R, Du P, Hu H, Wang T, Zhu L, Chen H (2014) Polyhedral $\text{LiNi}_{0.5}\text{Mn}_{1.5}\text{O}_4$ with excellent electrochemical properties for lithium-ion batteries. *J Mater Chem A* 2:12835–12848
- Wang J, Lin W, Wu B, Zhao J (2014) Porous $\text{LiNi}_{0.5}\text{Mn}_{1.5}\text{O}_4$ sphere as 5 V cathode material for lithium ion batteries. *J Mater Chem A* 2:16434–16442
- Zhang X, Cheng F, Yang J, Chen J (2013) $\text{LiNi}_{0.5}\text{Mn}_{1.5}\text{O}_4$ porous nanorods as high-rate and long-life cathodes for Li-ion batteries. *Nano Lett* 13:2822–2825
- Tang Y, Rui X, Zhang Y, Lim TM, Dong Z, Hng HH, Chen X, Yan Q, Chen Z (2013) Vanadium pentoxide cathode materials for high-performance lithium-ion batteries enabled by a hierarchical nanoflower structure via an electrochemical process. *J Mater Chem A* 1:82–88
- Lou XW, Archer LA, Yang Z (2009) ChemInform abstract: hollow micro-/nanostructures: synthesis and applications. *Adv Mater* 40:3987–4019
- X. Wang, J. Feng, Y. Bai, Q. Zhang, Y. Yin (2016) Synthesis, properties, and applications of hollow micro-/nanostructures, *Chem Rev.*116:10983
- Rui X, Tan H, Sim D, Liu W, Xu C, Hng HH, Yazami R, Lim TM, Yan Q (2013) Template-free synthesis of urchin-like Co_3O_4 hollow spheres with good lithium storage properties. *J Power Sources* 222:97–102
- Xue Y, Wang ZB, Zheng LL, Yu FD, Liu BS, Zhang Y, Zhou YX (2015) Synthesis and performance of hollow $\text{LiNi}_{0.5}\text{Mn}_{1.5}\text{O}_4$ with different particle sizes for lithium-ion batteries. *Rsc Advances* 5:100730–100735
- Wu WW, Xiang HF, Zhong GB, Su W, Tang W, Zhang Y, Yu Y, Chen CH (2014) Ordered $\text{LiNi}_{0.5}\text{Mn}_{1.5}\text{O}_4$ hollow microspheres as high-rate 5 V cathode materials for lithium ion batteries. *Electrochim. Acta* 119:206–213
- Seyyedhosseinzadeh H, Mahboubi F, Azadmehr A (2014) Estimation on diffusion coefficient of lithium ions at the interface of $\text{LiNi}_{0.5}\text{Mn}_{1.5}\text{O}_4$ /electrolyte in Li-ion battery. *Ionics* 21:335–344
- Schmok K, Bergakademie Freiberg SVU, Silikattechnik F (1988) DDR Modelling of mechanism of agglomeration of KC1 crystallization. *Cryst Res Technol* 8:967–972
- Zeng S, Ren G, Xu C, Yang Q (2011) High uniformity and monodispersity of sodium rare-earth fluoride nanocrystals: Controllable synthesis, shape evolution and optical properties. *CrystEngComm* 13:1384–1390
- Zhou L, Zhou X, Huang X, Liu Z, Zhao D, Yao X, Yu C (2013) Designed synthesis of LiMn_2O_4 microspheres with adjustable hollow structures for lithium-ion battery applications. *J Mater Chem A* 1:837–842
- Fang M, Tan X, Liu M, Kang S, Hu X, Zhang L (2011) Low-temperature synthesis of Mn_3O_4 hollow-tetraprism structures and their application in electrochemical capacitors. *CrystEngComm* 13:4915–4920
- Xu GL, Qin Y, Ren Y, Cai L, An K, Amine K, Chen Z (2015) The migration mechanism of transition metal ions in $\text{LiNi}_{0.5}\text{Mn}_{1.5}\text{O}_4$. *J Mater Chem A* 3:13031–13033
- Cui X, Li H, Li S (2017) Effects of different precipitants on $\text{LiNi}_{0.5}\text{Mn}_{1.5}\text{O}_4$, for lithium ion batteries prepared by modified co-precipitation method, *Ionics* 1–7
- Tu KN, Gösele U (2005) Hollow nanostructures based on the Kirkendall effect: design and stability considerations. *Appl Phys Lett* 86:711
- Xue Y, Wang ZB, Zheng LL (2015) Synthesis and performance of hollow $\text{LiNi}_{0.5}\text{Mn}_{1.5}\text{O}_4$ with different particle sizes for lithium-ion batteries. *Rsc Advances* 5:100730–100735